

# Millisecond pulsar interpretation of the Galactic center gamma-ray excess

Qiang Yuan<sup>a,b</sup>, Bing Zhang<sup>b</sup>

<sup>a</sup>*Key Laboratory of Particle Astrophysics, Institute of High Energy Physics, Chinese Academy of Science, Beijing 100049, P.R.China*

<sup>b</sup>*Department of Physics and Astronomy, University of Nevada Las Vegas, NV 89154, USA*

---

## Abstract

It was found in the Fermi-LAT data that there is an extended  $\gamma$ -ray excess in the Galactic center region. The proposed sources to be responsible for the excess include dark matter annihilation or an astrophysical alternative from a population of millisecond pulsars (MSPs). Whether or not the MSP scenario can explain the data self-consistently has very important implications for the detection of particle dark matter, which is however, subject to debate in the literature. In this work we study the MSP scenario in detail, based on the detected properties of the MSPs by Fermi-LAT. We construct a model of Milky Way disk-component MSPs which can reproduce the  $\gamma$ -ray properties of the observed Fermi-LAT MSPs, and derive the intrinsic luminosity function of the MSPs. The model is then applied to a bulge population of MSPs. We find that the extended  $\gamma$ -ray excess can be well explained by the bulge MSPs without violating the detectable flux distribution of MSPs by Fermi-LAT. The spatial distribution of the bulge MSPs as implied by the distribution of low mass X-ray binaries follows a  $r^{-2.4}$  profile, which is also consistent with the  $\gamma$ -ray excess data. We conclude that the MSP model can explain the Galactic center  $\gamma$ -ray excess self-consistently, satisfying all the current observational constraints.

---

## 1. Introduction

It has been reported that there is an extended  $\gamma$ -ray excess in the Galactic center (GC) region in the Fermi Large Area Telescope (Fermi-LAT) data [1, 2, 3, 4, 5, 6, 7, 8]. The spatial distribution of the extended excess follows the square of a generalized Navarro-Frenk-White (gNFW, [9, 10]) profile with

inner slope  $\gamma \approx 1.2$ , and the  $\gamma$ -ray spectrum can be fitted with an exponential cutoff power-law or a log-parabolic form [3, 5, 6]. The spatial extension of the excess is rather large. Daylan et al. found that up to  $12^\circ$  away from the GC the excess is still remarkable [8]. The analysis of the spatial variation of the  $\gamma$ -ray emission from the Fermi bubbles [11] showed that there might also be an extra component overlapping on the bubble emission, which follows the same projected gNFW<sup>2</sup> distribution of the GC excess [12, 13, 8]. This means the excess may exist at even larger scales.

The origin of this excess is still unclear, and the proposed sources include dark matter (DM) annihilation [14, 15, 16, 17, 18, 19, 20, 21] or a population of millisecond pulsars (MSPs, [22, 23], see also an earlier work on a MSP interpretation to EGRET diffuse  $\gamma$ -ray emission [24]). Although the DM scenario seems very attractive, it is very crucial to investigate the astrophysical alternatives of the excess, especially in view that direct detection experiments found no signal of DM collision in the corresponding mass ranges [25, 26]. A first look at the MSP scenario suggests that it is a plausible interpretation to the data. The best-fitting spectrum of the excess is an exponential cutoff power-law, with power law index  $\Gamma \sim 1.4 - 1.6$  and cutoff energy  $E_c \sim 3 - 4$  GeV [6, 27]. All these are consistent with the average spectral properties of either the Fermi-LAT detected MSPs [28], or globular clusters whose  $\gamma$ -ray emission is believed to be dominated by MSPs [29]. The number of MSPs needed to explain the data is estimated to be a few  $\times 10^3$  based on the observed luminosities of MSPs or globular clusters [5, 23, 6]. Such a number of MSPs is plausible based on the comparison of the stellar mass content in the Galactic bulge and in the globular clusters. The spatial distribution of the  $\gamma$ -ray excess follows a gNFW profile, which is somehow expected within the dark matter scenario according to N-body simulations with baryon processes [30, 31]. However, it is interesting to note that the number distribution of low mass X-ray binaries (LMXBs), which can be tracers of MSPs, from the central region of Andromeda gives a projected  $R^{-1.5}$  profile [32, 33], which is consistent with that to interpret the  $\gamma$ -ray excess [5].

Hooper et al. investigated in more detail of the MSP scenario to explain the GC excess [34]. Based on several assumptions about the spatial, spin and luminosity distributions of the MSPs, they claimed that MSPs cannot explain the  $\gamma$ -ray excess data without violating the Fermi-LAT detected number-flux distribution of the MSPs. We revisit this problem in this work, paying special attention on the assumption of the luminosity function of MSPs. We will model the spatial and spectral distribution of MSPs in the Milky Way (MW)

disk to reproduce the major MSP observational properties as measured by Fermi-LAT, and infer the intrinsic luminosity function of MSPs (Sec. 2). We then apply the intrinsic luminosity function to a putative bulge population of MSPs and work out their contribution to the diffuse  $\gamma$ -ray excess without over-producing detectable point sources above the sensitivity threshold of Fermi-LAT (Sec. 3). We show that the MSP scenario can nicely reproduce the  $\gamma$ -ray excess data, and conclude in Sec. 4 with some discussion.

## 2. Simulation of MW disk MSPs

We first try to reproduce the Fermi-LAT observations with a MW disk population of MSPs. In the second Fermi-LAT catalog of pulsars (2FPC), 117 pulsars were reported, among which 40 are MSPs with 37 having spectral measurements [28]. Additionally there are about 30 pulsars ( $\sim 20$  are MSPs) which were not included in the 2FPC and can be found in an online catalog<sup>1</sup>. Our analysis is based on the 37 MSPs in the 2FPC catalog.

### 2.1. Spatial distribution

The spatial distribution of the MW disk MSPs is adopted as [35]

$$n(r, z) \propto \exp(-r^2/2\sigma_r^2) \exp(-|z|/\sigma_z), \quad (1)$$

where  $r$  and  $z$  are cylindrical coordinates. The radial and vertical scales are adopted to be the “base model” of [35], with  $\sigma_r = 5$  kpc and  $\sigma_z = 1$  kpc. Our study is not very sensitive to the spatial distribution, thus we will fix these parameters in the following discussion.

### 2.2. Spectral distribution

The  $\gamma$ -ray photon spectrum of a MSP can be generally described with an exponential cut-off power-law function

$$dN/dE \propto E^{-\Gamma} \exp(-E/E_c). \quad (2)$$

Fig. 1 shows the distributions of  $\gamma$ -ray spectral indices  $\Gamma$ , cutoff energies  $E_c$  and  $\gamma$ -ray luminosities<sup>2</sup>  $L$  of the 2FPC MSPs [28]. In each panel we have a

---

<sup>1</sup><https://confluence.slac.stanford.edu/display/GLAMCOG/Public+List+of+LAT-Detected+Gamma-Ray+Pulsars>

<sup>2</sup>In this work the  $\gamma$ -ray luminosity and flux are computed between 100 MeV and 100 GeV, unless otherwise stated.

scatter plot to show the correlation between any pair of these parameters, and two histograms to show the distributions of each parameter.

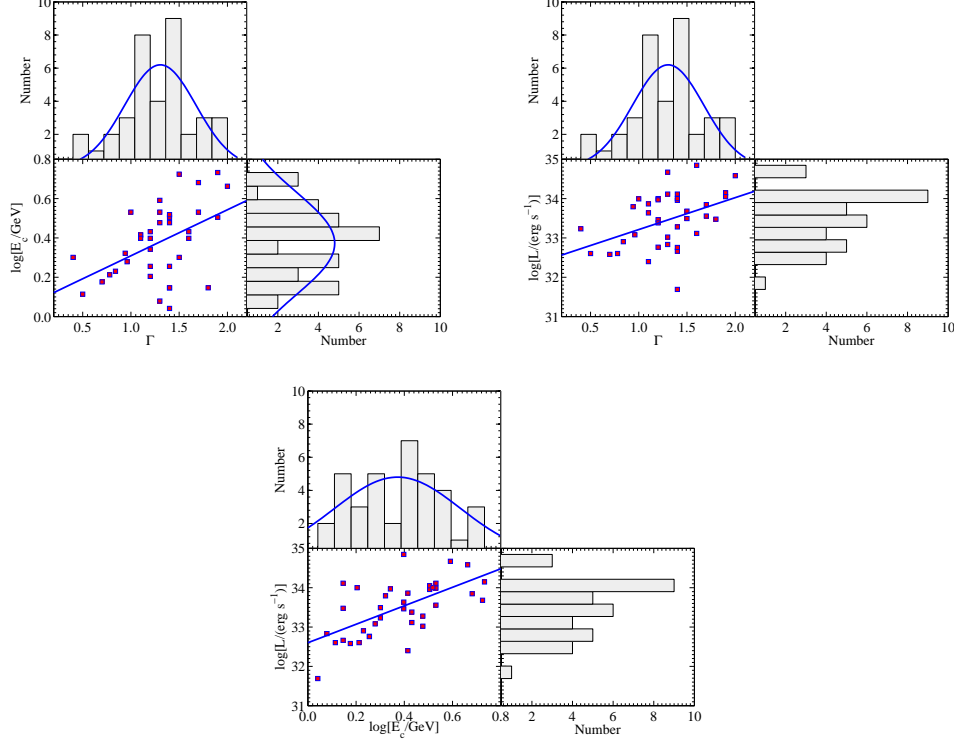


Figure 1: Distributions of  $\Gamma$ ,  $\log[E_c/\text{GeV}]$  and  $\log[L/\text{erg s}^{-1}]$  of the Fermi-LAT MSPs.

The distributions of  $\Gamma$  and  $\log[E_c/\text{GeV}]$  can be fitted with Gaussian functions (blue lines in the histograms). The mean value and width are found to be 1.305 and 0.370 for  $\Gamma$ , and 0.372 and 0.261 for  $\log[E_c/\text{GeV}]$ . We do not fit the luminosity distribution based on the observed sample because the observational selection effect may favor the detection of high luminosity ones. The intrinsic luminosity function can be only assumed and verified through the observations with a proper consideration of the detection selection effect. We also note that there might be some correlations among these parameters. Linear fittings to these correlations give

$$\begin{aligned}\log[E_c/\text{GeV}] &= 0.23\Gamma + 0.08, \\ \log[L/(\text{erg s}^{-1})] &= 0.81\Gamma + 32.42, \\ \log[L/(\text{erg s}^{-1})] &= 2.35 \log[E_c/\text{GeV}] + 32.58,\end{aligned}$$

but the correlations are weak due to large scatter. The Pearson's  $r$  values for the three pairs of parameters shown above are 0.47, 0.43 and 0.62, respectively. For simplicity we will neglect the correlations in most of the following discussion. However, the impacts of the correlations among these parameters will be tested in the end of Sec. 3. In the simulation as discussed below, we will further apply the following constraints on the spectral parameters:  $\Gamma > 0$  and  $1 \text{ GeV} < E_c < 10 \text{ GeV}$ .

### 2.3. Luminosity function

The luminosity function is most relevant for this study. However, it cannot be directly derived through the observational sample due to the sensitivity limit of the detectors. Hooper et al. assumed a power-law distribution of the MSP periods<sup>3</sup>  $dN/dP \propto P^{-2}$ , and a constant fraction of the spin-down power goes into  $\gamma$ -ray luminosities  $L_\gamma \propto \dot{E}$  [34]. For a constant magnetic field  $B$  one has  $\dot{E} \propto P^{-4}$ , and the luminosity function is  $dN/dL \propto L^{-3/4}$ . A log-normal distribution of the magnetic field of MSPs is assumed [34], and the resulting luminosity function can be derived through a Monte Carlo simulation. An example adopted in [34], with a central value of magnetic field  $B_0 = 10^{8.5} \text{ G}$  and a logarithmic standard width 0.2, is shown by the dashed line in Fig. 2. We see that such a luminosity function is very hard, which might be the reason why Hooper et al. did not find enough contribution from low-luminosity MSPs to explain the observed  $\gamma$ -ray excess [34].

However, we find that such a luminosity function may be over hard. If we accept such a luminosity function, and apply the detection threshold condition<sup>4</sup>  $F(> \text{GeV}) > 4 \times 10^{-10} \text{ cm}^{-2} \text{ s}^{-1}$ , we find that  $\sim 40$  sources could be detected by Fermi-LAT as individual MSPs. The luminosities of those 40 sources are mainly above  $10^{34} \text{ erg s}^{-1}$  (dashed histogram in the inset of Fig. 2), which cannot reproduce the  $L$  distribution of the observed MSP population (solid, red histogram in the inset of Fig. 2). This suggests that the assumed luminosity function is too hard. We then introduce a softer luminosity function. We assume a broken power-law form of the luminosity

---

<sup>3</sup>As shown in Sec. 2.5 below, the  $dN/dP$  dependence would significantly affect the shape of luminosity function. This particular form lacks a physical justification, and cannot account for the observed  $P$  distribution of MSPs.

<sup>4</sup>Flux calculated assuming a unified  $\gamma$ -ray energy spectrum  $dN/dE_\gamma \propto E_\gamma^{-1.46} \exp(-E_\gamma/3.3 \text{ GeV})$ .

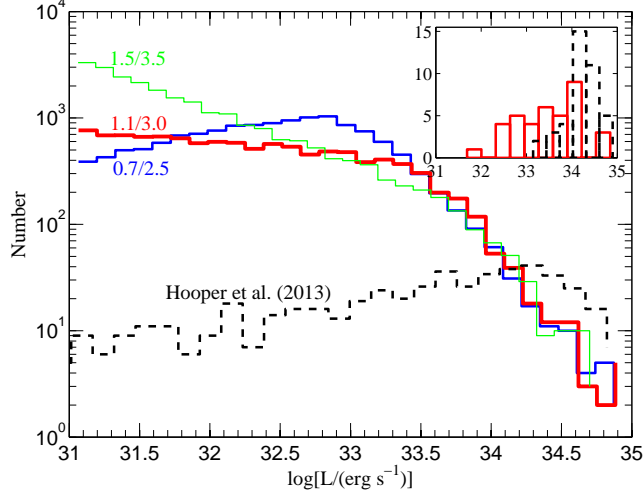


Figure 2: Gamma-ray luminosity function (proportional to  $dN/d\log L$ ) of MSPs. Solid lines are the broken power-law functions assumed in this work for several different sets of parameters as labelled, and the dashed line is an example as adopted in [34] with  $B_0 = 10^{8.5}\text{G}$ . The total number of the sources of each model is normalized to reproduce the observed sample. Inserted is a comparison of the luminosity distributions of the Fermi sample (red-solid line) and the expectation from the luminosity function given in [34] (black-dashed line). See the text for details.

function

$$dN/dL \propto L^{-\alpha_1} \left[ 1 + (L/L_{\text{br}})^2 \right]^{(\alpha_1 - \alpha_2)/2}. \quad (3)$$

The parameters  $\alpha_1$ ,  $\alpha_2$ ,  $L_{\text{br}}$  and the normalization are free parameters, which are determined by reproducing the observed sample of MSPs by Fermi-LAT. To compare with the Fermi-LAT detectability, we apply a latitude dependent sensitivity of Fermi-LAT as  $F_{\text{th}}(> 100 \text{ MeV}) = [2.0 \exp(-|b|/10^\circ) + 0.4] \times 10^{-8} \text{ cm}^{-2} \text{ s}^{-1}$ , which approximately accounts for the effect of the Galactic diffuse background on the point source sensitivity [36]. Here we adopt a one-year sensitivity of Fermi-LAT, although the 2FPC catalog was based on three-year observations. In principle, the sensitivity of Fermi-LAT would be better for a pulsar-like spectrum, which is harder than the  $E^{-2}$  spectrum used to derive the above point source sensitivity [28]. On the other hand, identifying a MSP would be challenging if the flux is just above the sensitivity threshold, since enough photons are needed to conduct MSP timing studies. The flux limit of identified MSPs is somewhat higher than the point source detection sensitivity, and we adopt a more conservative detection threshold to mimic

the threshold for identifying a MSP. This adopted detection threshold is also close to the upper edge of the three-year sensitivity bands for point sources with pulsar-like spectrum given in Fig. 17 of [28].

#### 2.4. Results

With the above mentioned spatial distribution, spectral distribution and luminosity function, we can simulate MSPs in the MW disk. The number of the simulated sources is normalized to reproduce the detected number of MSPs with fluxes (above 100 MeV) larger than  $F_{\text{th}}(b)$ . The results from one realization with luminosity function parameters  $\alpha_1/\alpha_2 = 1.1/3.0$  and  $L_{\text{br}} = 4 \times 10^{33} \text{ erg s}^{-1}$  are shown in Fig. 3. The top-left panel shows the sky distribution, and other panels show the distributions of distance  $d$ , luminosity  $L$  and flux  $F$ , respectively. In each panel, the black crosses represent the full simulated sample, the blue dots are the simulated sample with fluxes above  $F_{\text{th}}$ , and the red squares are Fermi-LAT detected sample. The distributions of  $\log d$ ,  $\log L$  and  $\log F$  are shown by the histograms in the rest three panels for the simulated high flux sample and the Fermi-LAT sample. We can see from this figure that the model can roughly reproduce the Fermi-LAT observations. To be more quantitative, we check the consistency between the simulated sample and the observed sample using the Kolmogorov-Smirnov test method. The probabilities that these two samples come from the same distributions are about 0.49, 0.93 and 0.44 for the distance, luminosity and flux distributions, respectively. The total number of the MW MSPs in this simulation is  $\sim 6000$  for  $L > 10^{32} \text{ erg s}^{-1}$ , which gives  $\sim 40$  detectable sources.

Due to the limited statistics of the observed sample, the model parameters cannot be precisely determined. We have tested other parameters and find that changing the luminosity function parameters  $\alpha_1/\alpha_2$  from 0.7/2.5 to 1.5/3.5 (accordingly  $L_{\text{br}}$  changes from  $1.0 \times 10^{33}$  to  $1.0 \times 10^{34} \text{ erg s}^{-1}$ ) would not significantly affect the model results. The observational distributions can all be approximately reproduced, even though the overall agreement becomes worse than the best fit results. The parameters of some luminosity function models are listed in Table 1, and the three example luminosity functions are plotted in Fig. 2. Compared with the luminosity function adopted in [34], our derived luminosity functions give many more low-luminosity sources, which would contribute significantly to the unresolved diffuse emission.

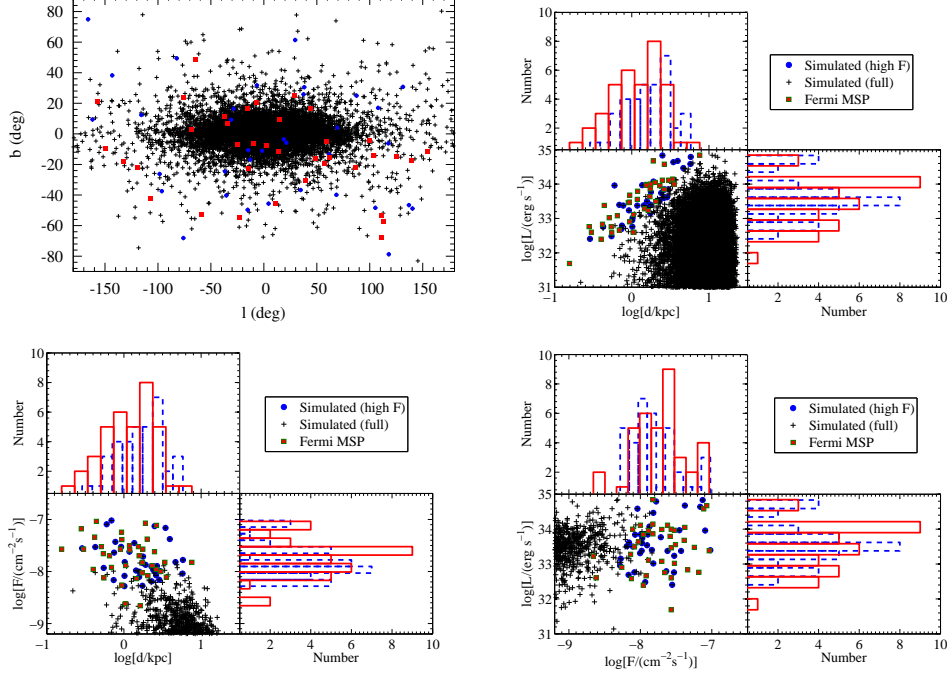


Figure 3: Comparisons of the spatial distribution, distances, luminosities and fluxes of MSPs between the simulated sample and the Fermi-LAT detected sample. The black crosses are the full simulated sample, the blue dots are the high-flux ones with  $F > F_{\text{th}}$ , and the red squares are Fermi-LAT detected sample. Histograms in the last three panels show the distributions of related quantities for the simulated high flux sample (blue dashed) and the Fermi-LAT sample (red solid).

Table 1: Parameters adopted in the simulation.

$\alpha_1/\alpha_2$	$L_{\text{br}}$ ( $10^{33} \text{ erg s}^{-1}$ )	$N_{\text{MW}}^a$	$N_{\text{bulge}}^a$
0.7/2.5	1.0	9000	17000
1.1/3.0	4.0	6000	13000
1.5/3.5	10.0	8000	16000

<sup>a</sup>Number with  $L$  between  $10^{32}$  and  $10^{35} \text{ erg s}^{-1}$ .

### 2.5. Physical interpretation of the luminosity function

We have shown that with a broken power-law form of the intrinsic luminosity function Eq. (3) and a proper consideration of the detection threshold,



the observational properties of the MW disk MSPs can be well reproduced. It is, however, necessary to justify that such a luminosity function is reasonable in realistic MSP models. Many theoretical models have been proposed to interpret the  $\gamma$ -ray emission from pulsars, including the polar cap model [37], outer gap model [39], slot gap model [40], pair starved polar cap model [38], two-pole caustic model [41], and annular ring model [42]. A recent study of the  $\gamma$ -ray light curves of MSPs seems to favor the outer gap model or two-pole caustic model, although other models may also work for some cases [43]. In this work we do not get into the detailed emission models of MSPs. Rather, we perform a phenomenological model to study the statistical properties of the  $\gamma$ -ray MSPs. As shown below, the intrinsic luminosity function does not sensitively depend on detailed emission models.

One can write the intrinsic luminosity function in the form

$$\frac{dN}{dL} = \frac{dN}{dP} \cdot \frac{dP}{d\dot{E}} \cdot \frac{d\dot{E}}{dL}. \quad (4)$$

We can see that it depends on the period distribution  $dN/dP$ , period-dependent spin-down luminosity  $dP/d\dot{E}$ , and the fraction of spin-down luminosity that goes to the observed  $\gamma$ -ray luminosity  $d\dot{E}/dL$ . Taking roughly a constant magnetic field strength for MSPs (so that  $\dot{E} \propto P^{-4}$ ), and assuming  $L \propto \dot{E}^a$  and  $dN/dP \propto P^b$  ( $b = -2$  as adopted in [34]), it is straightforward to derive

$$\frac{dN}{dL} \propto L^{-\frac{(b+1)}{4a}-1}. \quad (5)$$

Therefore the indices  $a$  and  $b$  determines the power law index of the luminosity function. The slope of luminosity function is much more sensitive to  $b$  than to  $a$ .

The  $L - \dot{E}$  relation depends on pulsar emission models, see e.g. [44] for polar cap models and [45] for outer gap models. In general,  $a$  is in the range of  $0.5 - 1$ . If the index  $b$  is a constant, one cannot reproduce the required broken power-law luminosity function for typical values of  $a$  (due to the insensitivity of the results on  $a$ ).

The results are more sensitive to  $b$ . If all the MSPs reach the “spin-up” limit and then spin-down, we may expect  $b = 1$  if the birth rate  $\dot{N}$  is constant<sup>5</sup>. However, observationally we do not see such a behavior. Neither

---

<sup>5</sup>For  $\dot{N} = C$ ,  $N \propto \tau \propto P/\dot{P} \propto P^2$  if  $B$  is constant.

do we see the  $b = -2$  behavior introduced by [34]. Rather, observationally, the period distribution of MSPs is not a single power-law. It has a peak around  $\sim 3 - 4$  ms. The deficiency of MSPs with even shorter periods is not due to a selection effect, since they have an even larger  $\dot{E}$  and should be more easily detected if they do exist. Therefore the break in the  $dN/dP$  distribution is intrinsic, and it naturally introduces a break in the intrinsic luminosity function of MSPs. Physically, there is a maximum spin frequency at birth for MSPs, defined by the so-called “spin-up” line, at which the accretion from the companion can no longer transfer angular momentum to the pulsar (the shortest period of pulsars to date is 1.4 ms [46]). Introducing a distribution of magnetic field strength and a distribution of the “ending time” during the spin-up phase for MSPs at birth would naturally give rise to a peak in the  $P$  distribution. We note that for a typical value  $B \sim 10^{8.5}$  G, such a peak period corresponds to a spin-down power  $(1.5 - 5) \times 10^{34}$  erg s $^{-1}$ . If the  $\gamma$ -ray luminosity of MSPs shares a few percent of  $\dot{E}$ , it would correspond to a break of the luminosity function at  $10^{33}$  erg s $^{-1}$ , which is the one required in our modeling.

The slopes  $\alpha_1$  and  $\alpha_2$  can be determined by the parameters  $a$  and  $b$ . We adopt power-law fits to approximate the period distribution below and above the peak period<sup>6</sup>  $P_{\text{br}}$ . We have  $b \approx -2$  for  $P > P_{\text{br}}$ , and  $b \approx 2 - 3$  for  $P < P_{\text{br}}$ . In the low-luminosity regime ( $P > P_{\text{br}}$ ), usually  $a \approx 1$ . This gives  $\alpha_1 \sim 0.75$ . In the high-luminosity regime ( $P < P_{\text{br}}$ ), one has  $a \approx 0.5 - 1$  [44, 45]. This gives  $\alpha_2 \approx 1.75 - 3$ . These values of  $\alpha_1$  and  $\alpha_2$  are close to those adopted in Sec. 2.4 in order to reproduce the Fermi-LAT observations.

### 3. Simulation of bulge MSPs

The Galactic bulge is rich in stars, hence also rich in remnants of stars, i.e., compact objects such as black holes and neutron stars. The number of compact objects is estimated to be  $\sim 20000$  in the inner pc region [47, 48]. The number of compact objects should be much more within the kpc scale, which is relevant to this study. Furthermore, the high number density of stars in the Galactic bulge facilitates the dynamic formation of binary systems [32, 33], which are progenitors of MSPs. In this section we model the MSP population in the Galactic bulge, based on the spectral parameters and

---

<sup>6</sup>The distribution may also be fitted as a Gaussian distribution (e.g., [24]).

luminosity function derived in Sec. 2. We will investigate their contribution to the GC  $\gamma$ -ray excess without over-predicting detectable sources by Fermi-LAT.

### 3.1. Spatial distribution

MSPs are believed to be recycled pulsars born in binary systems. The LMXBs are considered as progenitor of MSP systems, and are believed to trace the distribution of MSPs [49]. The observational surface density profile of resolved LMXBs in the center of M 31 (at sub-kpc scale) traces the stellar mass profile at a scale larger than  $1'$ , and shows a significant “excess” in the inner arc-minute region [32]. The inner “excess” can be explained by the dynamic formation scenario of LMXBs through stellar encounters in a very high stellar density environment [33]. The overall surface density profile of LMXBs can be approximated with a  $\theta^{-1.5}$  behavior, which is consistent with the projected profile of the  $\gamma$ -ray excess in the GC region [5].

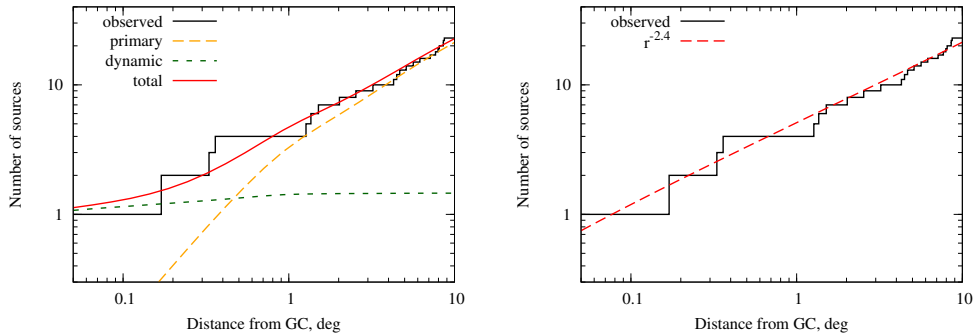


Figure 4: Left: spatial distribution of the MW transient LMXBs [50], compared with the prediction from the stellar mass distribution. The primary term is proportional to  $\rho_*$  and the dynamic term is proportional to  $\rho_*^2$  [32, 33]. Right: spatial distribution of the MW LMXBs compared with a  $r^{-2.4}$  distribution which mimics the generalized-NFW square profile with inner slope  $\gamma = 1.2$ .

The distribution of MW LMXBs is less well constrained. Revnivtsev et al. reported a number of LMXBs within the central 10 degrees of the MW [50]. The cumulative number of transient LMXBs also shows an increase in the innermost region compared with the stellar mass distribution  $\rho_*$ . We show that the model prediction can well reproduce the data by adding a dynamic term which is proportional to  $\rho_*^2$ , as shown in the left panel of Fig. 4. The stellar mass model we use is the same as that used in [50]. In the right

panel of Fig. 4 we show the expected cumulative distribution of LMXBs for a  $r^{-2.4}$  profile as indicated by the GeV  $\gamma$ -ray excess, where  $r$  is the spherical coordinate. It is intriguing to see that the observed spatial distribution of LMXBs can be also nicely fitted by the  $r^{-2.4}$  generalized NFW profile. This suggests that an apparent generalized NFW profile does not necessarily mean a dark matter signature.

For simplicity in the following we assume a spherically symmetric distribution with spatial profile  $r^{-2.4}$  of MSPs in the bulge. Note that if the stellar model of LMXB formation is correct, there should be an asymmetry in the MSP distribution, with a tendency to elongate along the Galactic longitude. According to the observed LMXB sample, there is no such elongation at least for the the central  $1.3^\circ$  away from the GC [50]. For a better determination of the density profile of MSPs, we need a larger sample of LMXBs. On the other hand, the search for asymmetry of the GC  $\gamma$ -ray excess cannot exclude a weak elongation along the Galactic plane, although no significant asymmetry was found [8]. This means that even if the MSP distribution is slightly asymmetric, it may also be consistent with the morphology of the observed  $\gamma$ -ray excess. The simulated spatial distribution of the bulge MSPs is shown in Fig. 5. Note here we additionally apply a truncation of the density profile for  $\theta > 10^\circ$ , which may represent the size of the bulge.

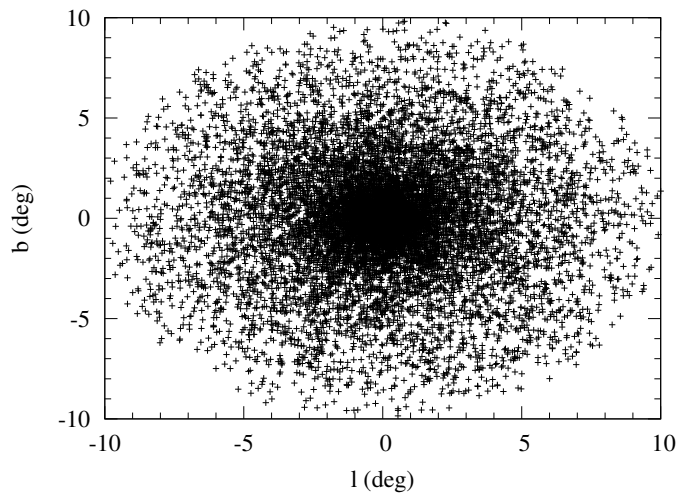


Figure 5: Simulated spatial distribution of the bulge MSPs.

### 3.2. Spectral distribution

Finally we compare the expected  $\gamma$ -ray spectrum from the population of bulge MSPs with the Fermi-LAT GC excess. The cumulative flux from the MSP population depends on the number of MSPs, which is adjusted to match the  $\gamma$ -ray excess data [6]. Fig. 6 shows the result for the model with the luminosity function parameters  $\alpha_1/\alpha_2 = 1.1/3.0$  as given in Table 1. To compare with the data, only the MSPs that lie within the  $7^\circ \times 7^\circ$  box centered on GC are employed. It is not surprising that the model can well reproduce the data, because the average energy spectra of MSPs are consistent with the  $\gamma$ -ray excess data. It also shows that for this luminosity function the MSPs with luminosities between  $10^{33}$  and  $10^{34}$   $\text{erg s}^{-1}$  contribute dominantly to the total flux. This is reasonable because the break of the luminosity function lies in this luminosity range. The number of MSPs needed to give enough cumulative flux to explain the data is estimated to be  $\sim 13000$  for  $L > 10^{32}$   $\text{erg s}^{-1}$ . Obviously such a number depends on the lower cutoff of the luminosity function. For the other two luminosity functions in Table 1 we have similar results, with quantitatively different number of sources and weights among different luminosity ranges.

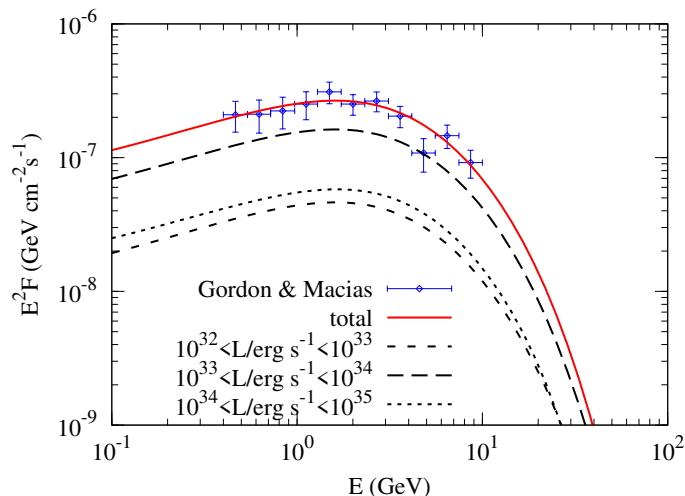


Figure 6: Cumulative spectrum of the bulge MSPs compared with the Fermi-LAT GC excess data [6].

In order to check whether the bulge MSP population violates the Fermi-LAT observations, we show the fluxes versus luminosities of these MSPs in

Fig. 7. The vertical line is the sensitivity of Fermi-LAT for sources located in the Galactic plane [36]. It is shown that none of these bulge MSPs could be detected as an individual source by Fermi-LAT, which means that all of them should contribute to the diffuse emission.

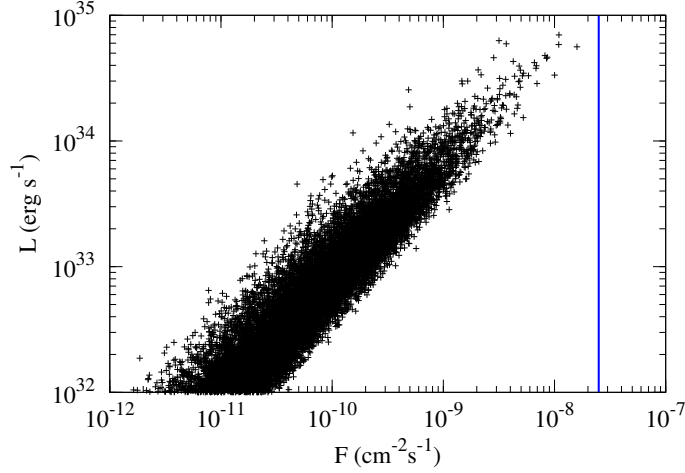


Figure 7: Simulated  $F$  vs.  $L$  distributions of the bulge MSPs. The vertical line is the sensitivity of Fermi-LAT for sources located in the Galactic plane [36].

We can compare the number of MSPs estimated here with that derived in other works. Using the average luminosity of the Fermi-LAT detected MSPs,  $\bar{L} \approx 10^{34} \text{ erg s}^{-1}$ , Macias & Gordon estimated a number of  $\sim 1000$  MSPs in order to explain the data [27]. This number should be a lower bound because there should be more low-luminosity MSPs which are not detected. In our work, the main contribution to the total  $\gamma$ -rays comes from the MSPs with luminosities between  $10^{33}$  and  $10^{34} \text{ erg s}^{-1}$  (Fig. 6). We find that the number of MSPs in this luminosity range is about 4200 for a total number of 13000 ( $L > 10^{32} \text{ erg s}^{-1}$ ). If we count only the  $7^\circ \times 7^\circ$  box the number becomes 2700, which is consistent with the lower limit derived in [27], given the average luminosity is about several times smaller. However, as we have mentioned, this number depends on how many low-luminosity MSPs there are. There is only one MSP with luminosity below  $10^{32} \text{ erg s}^{-1}$  in the Fermi-LAT sample, but we are not sure whether the luminosity function can extend to even lower luminosities or not. If so the number of MSPs may be even larger than that given in Table 1.

Finally we test the model with the correlations between spectral parameters and luminosity. We employ a simple approach to approximate the correlations between  $L$  and the spectral parameters shown in Fig. 1: for  $10^{32} < L < 10^{33} \text{ erg s}^{-1}$ ,  $\langle \Gamma \rangle = 1.0$ ,  $\langle \log[E_c/\text{GeV}] \rangle = 0.2$ , for  $10^{33} < L < 10^{34} \text{ erg s}^{-1}$ ,  $\langle \Gamma \rangle = 1.3$ ,  $\langle \log[E_c/\text{GeV}] \rangle = 0.4$ , and for  $10^{34} < L < 10^{35} \text{ erg s}^{-1}$ ,  $\langle \Gamma \rangle = 1.6$ ,  $\langle \log[E_c/\text{GeV}] \rangle = 0.6$ , respectively. Here the angle brackets  $\langle \dots \rangle$  denote the average value of corresponding quantities. The widths of  $\Gamma$  and  $\log[E_c/\text{GeV}]$  are kept unchanged. The result for the same model as that in Fig. 6 is shown in Fig. 8. Since the MSPs with  $10^{33} < L < 10^{34} \text{ erg s}^{-1}$  dominate the contribution, the total spectrum do not change significantly compared with that when the correlations are not taken into account.

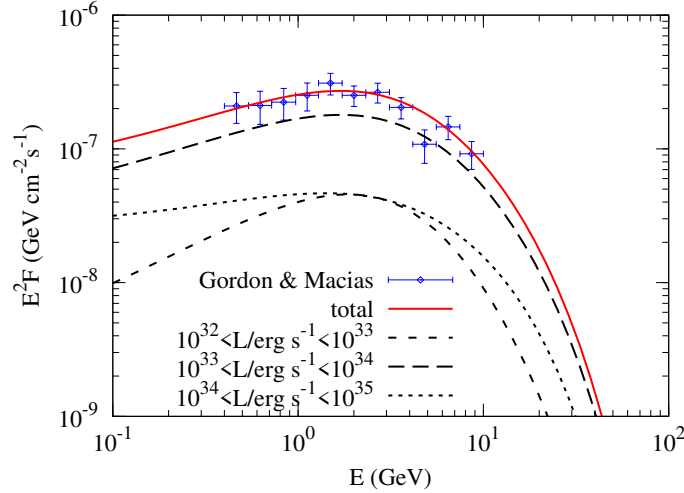


Figure 8: Same as Fig. 6 but the correlations between  $L$  and  $\Gamma$ ,  $L$  and  $E_c$  are included. See the text for details.

#### 4. Conclusion and discussion

The analysis of the Fermi-LAT data revealed symmetric and extended  $\gamma$ -ray excess in the GC region peaking at GeV energies [1, 2, 3, 4]. The origin of the excess is not clear, and the promising scenarios include DM annihilation and an unresolved MSP population. Although the spectrum of the  $\gamma$ -ray excess is quite consistent with the average spectrum of the Fermi-LAT detected MSPs, it was argued that in order not to over-produce the

detectable MSPs by Fermi-LAT, the unresolved MSP population can only account for  $\lesssim 10\%$  of the observed  $\gamma$ -ray [34].

In this work we study the MSP scenario in detail, by including more comprehensive observational constraints from the observational properties of the Fermi-LAT detected MSP sample. We find that there is a large uncertainty in the intrinsic  $\gamma$ -ray luminosity function of MSPs, which affects significantly the prediction of the diffuse emission from the unresolved MSP population. It was found that the luminosity function adopted in [34] might be too hard to reproduce the observed luminosity function of the Fermi-LAT MSP sample. Adjusting properly the intrinsic luminosity function we can well reproduce the observational properties of the Fermi-LAT MSPs with the MW population of MSPs. Based on this refined luminosity function, we find that a population of MSPs in the bulge can be enough to explain the  $\gamma$ -ray excess without over-producing the detectable MSPs above the sensitivity of Fermi-LAT. The number of MSPs with luminosities higher than  $10^{32} \text{ erg s}^{-1}$  in the whole bulge region is estimated to be  $(1 - 2) \times 10^4$  in order to explain the  $\gamma$ -ray data. Such a number is compatible with the estimate of the compact remnants in the very central region around the GC [47, 48].

We further investigate the spatial distribution of the bulge MSP population, using LMXBs as tracers. Assuming a spatial density profile of  $r^{-2.4}$  we can well reproduce the observed LMXB distribution within  $10^\circ$  around the GC [50]. Such a density profile is quite consistent with that required to explain the GC  $\gamma$ -ray excess. However, we still need to keep in mind that the current constraint on the number density profile of LMXBs in the GC region is poor. It is possible that the density profile of LMXBs is slightly elongated along the Galactic plane as expected from the stellar model. In that case the MSP scenario may have some tension with the  $\gamma$ -ray data [8].

We show in this work that the MSP population can naturally explain the  $\gamma$ -ray excess in the GC region. It should be pointed out that any other astrophysical populations with similar spectral, luminosity and spatial characteristics as the MSPs could also be the origin of the excess. In any case, MSPs are the most natural sources to satisfy these constraints.

We note that some analyses claimed the  $\gamma$ -ray excesses extend to even larger scales in the inner Galaxy [12, 13, 8]. The excess spectra in these regions seem to be even harder than that in the GC, and may be difficult to be explained by MSPs [34]. However, the analysis at large scales may suffer from uncertainties from the large scale diffuse background subtraction, especially if the emission from the Fermi bubbles is not uniform [51]. In spite



that there are also uncertainties from the diffuse backgrounds, the results from the GC analysis seem to be more robust [6, 27]. Nevertheless, if the  $\gamma$ -ray excess does extend to larger scales ( $\gg 10^\circ$  from GC), the MSP scenario may face difficulty.

Finally we propose that multi-wavelength observations of the counterpart of the  $\gamma$ -ray excess, in e.g. X-rays, may help verify its existence as well as identify its nature. The X-ray emission from the MSPs and possibly the binary systems may show different properties (flux, skymap and spectrum) compared with that from DM annihilation, which could be detectable by e.g., NuSTAR and other future X-ray missions.

## Acknowledgments

We thank X.-J. Bi, Y.-Z. Fan, A. Harding, L. Ho, D. Hooper, T. Linden, T. P. H. Tam and W. Wang for valuable comments and discussion. This work is supported by 973 Program under Grant No. 2013CB837000, and by National Natural Science Foundation of China under Grant No. 11105155 (for QY).

## References

- [1] L. Goodenough and D. Hooper, ArXiv e-prints:0910.2998 (2009), 0910.2998.
- [2] V. Vitale, A. Morselli, and for the Fermi/LAT Collaboration, ArXiv e-prints:0912.3828 (2009), 0912.3828.
- [3] D. Hooper and L. Goodenough, Physics Letters B **697**, 412 (2011), 1010.2752.
- [4] A. Boyarsky, D. Malyshev, and O. Ruchayskiy, Physics Letters B **705**, 165 (2011), 1012.5839.
- [5] K. N. Abazajian and M. Kaplinghat, Phys. Rev. D **86**, 083511 (2012), 1207.6047.
- [6] C. Gordon and O. Macías, Phys. Rev. D **88**, 083521 (2013), 1306.5725.
- [7] K. N. Abazajian, N. Canac, S. Horiuchi, and M. Kaplinghat, ArXiv e-prints:1402.4090 (2014), 1402.4090.

- [8] T. Daylan, D. P. Finkbeiner, D. Hooper, T. Linden, S. K. N. Portillo, N. L. Rodd, and T. R. Slatyer, ArXiv e-prints:1402.6703 (2014), 1402.6703.
- [9] J. F. Navarro, C. S. Frenk, and S. D. M. White, *Astrophys. J.* **490**, 493 (1997), astro-ph/9611107.
- [10] H. Zhao, *Mon. Not. Roy. Astron. Soc.* **278**, 488 (1996), astro-ph/9509122.
- [11] M. Su, T. R. Slatyer, and D. P. Finkbeiner, *Astrophys. J.* **724**, 1044 (2010), 1005.5480.
- [12] D. Hooper and T. R. Slatyer, *Physics of the Dark Universe* **2**, 118 (2013), 1302.6589.
- [13] W.-C. Huang, A. Urbano, and W. Xue, ArXiv e-prints:1307.6862 (2013), 1307.6862.
- [14] D. Hooper and T. Linden, *Phys. Rev. D* **84**, 123005 (2011), 1110.0006.
- [15] G. Marshall and R. Primulando, *Journal of High Energy Physics* **5**, 26 (2011), 1102.0492.
- [16] G. Zhu, *Phys. Rev. D* **83**, 076011 (2011), 1101.4387.
- [17] W.-C. Huang, A. Urbano, and W. Xue, ArXiv e-prints:1310.7609 (2013), 1310.7609.
- [18] K. Prasad Modak, D. Majumdar, and S. Rakshit, ArXiv e-prints (2013), 1312.7488.
- [19] C. Boehm, M. J. Dolan, C. McCabe, M. Spannowsky, and C. J. Wallace, ArXiv e-prints:1401.6458 (2014), 1401.6458.
- [20] T. Lacroix, C. Boehm, and J. Silk, ArXiv e-prints:1403.1987 (2014), 1403.1987.
- [21] P. Agrawal, B. Batell, D. Hooper, and T. Lin, ArXiv e-prints:1404.1373 (2014), 1404.1373.
- [22] K. N. Abazajian, *J. Cosmol. Astropart. Phys.* **3**, 010 (2011), 1011.4275.

- [23] N. Mirabal, Mon. Not. Roy. Astron. Soc. **436**, 2461 (2013), 1309.3428.
- [24] W. Wang, Z. J. Jiang, and K. S. Cheng, Mon. Not. Roy. Astron. Soc. **358**, 263 (2005), astro-ph/0501245.
- [25] E. Aprile, et al., Physical Review Letters **109**, 181301 (2012), 1207.5988.
- [26] D. S. Akerib, et al., Physical Review Letters **112**, 091303 (2014), 1310.8214.
- [27] O. Macias and C. Gordon, Phys. Rev. D **89**, 063515 (2014), 1312.6671.
- [28] A. A. Abdo, et al., Astrophys. J. Supp. **208**, 17 (2013), 1305.4385.
- [29] A. A. Abdo, et al., Astron. Astrophys. **524**, A75 (2010).
- [30] O. Y. Gnedin, A. V. Kravtsov, A. A. Klypin, and D. Nagai, Astrophys. J. **616**, 16 (2004), astro-ph/0406247.
- [31] O. Y. Gnedin, D. Ceverino, N. Y. Gnedin, A. A. Klypin, A. V. Kravtsov, R. Levine, D. Nagai, and G. Yepes, ArXiv e-prints:1108.5736 (2011), 1108.5736.
- [32] R. Voss and M. Gilfanov, Astron. Astrophys. **468**, 49 (2007), astro-ph/0610649.
- [33] R. Voss and M. Gilfanov, Mon. Not. Roy. Astron. Soc. **380**, 1685 (2007), astro-ph/0702580.
- [34] D. Hooper, I. Cholis, T. Linden, J. M. Siegal-Gaskins, and T. R. Slatyer, Phys. Rev. D **88**, 083009 (2013), 1305.0830.
- [35] C.-A. Faucher-Giguère and A. Loeb, J. Cosmol. Astropart. Phys. **1**, 005 (2010), 0904.3102.
- [36] W. B. Atwood, et al., Astrophys. J. **697**, 1071 (2009), 0902.1089.
- [37] J. K. Daugherty and A. K. Harding, Astrophys. J. **458**, 278 (1996), astro-ph/9508155.
- [38] A. G. Muslimov and A. K. Harding, Astrophys. J. **617**, 471 (2004), astro-ph/0408377.

- [39] K. S. Cheng, C. Ho, and M. Ruderman, *Astrophys. J.* **300**, 500 (1986).
- [40] A. G. Muslimov and A. K. Harding, *Astrophys. J.* **606**, 1143 (2004), [astro-ph/0402462](#).
- [41] J. Dyks and B. Rudak, *Astrophys. J.* **598**, 1201 (2003), [astro-ph/0303006](#).
- [42] G. J. Qiao, K. J. Lee, H. G. Wang, R. X. Xu, and J. L. Han, *Astrophys. J. Lett.* **606**, L49 (2004), [astro-ph/0403398](#).
- [43] T. J. Johnson, et al., *ArXiv e-prints*:1404.2264 (2014), [1404.2264](#).
- [44] A. K. Harding, A. G. Muslimov, and B. Zhang, *Astrophys. J.* **576**, 366 (2002), [astro-ph/0205077](#).
- [45] K. Hirotani, *Astrophys. J.* **766**, 98 (2013), [1301.5717](#).
- [46] J. W. T. Hessels, S. M. Ransom, I. H. Stairs, P. C. C. Freire, V. M. Kaspi, and F. Camilo, *Science* **311**, 1901 (2006), [astro-ph/0601337](#).
- [47] J. Miralda-Escudé and A. Gould, *Astrophys. J.* **545**, 847 (2000), [astro-ph/0003269](#).
- [48] P. Deegan and S. Nayakshin, *Mon. Not. Roy. Astron. Soc.* **377**, 897 (2007), [astro-ph/0611524](#).
- [49] D. Bhattacharya, in *IAU Colloq. 160: Pulsars: Problems and Progress*, edited by S. Johnston, M. A. Walker, and M. Bailes (1996), vol. 105 of *Astronomical Society of the Pacific Conference Series*, p. 547.
- [50] M. Revnivtsev, A. Lutovinov, E. Churazov, S. Sazonov, M. Gilfanov, S. Grebenev, and R. Sunyaev, *Astron. Astrophys.* **491**, 209 (2008), [0805.0259](#).
- [51] R.-z. Yang, F. Aharonian, and R. Crocker, *ArXiv e-prints*:1402.0403 (2014), [1402.0403](#).